Supplement of Atmos. Chem. Phys., 22, 12803–12825, 2022
https://doi.org/10.5194/acp-22-12803-2022-supplement

Atmospheric Chemistry and Physics
Open Access
EGU

Supplement of

Aerosol size distribution changes in FIREX-AQ biomass burning plumes: the impact of plume concentration on coagulation and OA condensation/evaporation

Nicole A. June et al.

Correspondence to: Nicole A. June (nicole.june@colostate.edu) and Jeffrey R. Pierce (jeffrey.pierce@colostate.edu)

Tables: 3
Figures: 19

Table S1: Relationship between $\sigma_\theta$and σ_ϕ and stability class. Where $\sigma_\theta = \frac{\sigma_v}{\bar{u}}$ and $\sigma_\phi = \frac{\sigma_w}{\bar{u}}$
Source: (Arya, 1999)

Stability Class	σ_θ [deg.]	σ_ϕ [deg.]
A	≥ 22.5	≥ 11.5
B	17.5 - 22.5	10.0 - 11.5
C	12.5 - 17.5	7.8 - 10.0
D	7.5 - 12.5	5.0 - 7.8
E	3.8 - 7.5	2.4 -5.0
F	< 3.8	< 2.4

Table S2: The age of the youngest sampled transect, the selected transect used for initializing the simulations in our study, and the reason for modification for each of the eight samplings.

Sampling	Sampled Youngest Age [h]	Selected Initialization Age [h]	Reason
7/25	0.25	0.75	First 5 sampled transects had a linear decrease in ln(ΔCO) (7.7 to 6.4), then increased to 8.1 before starting to linearly decrease again. More transects follow the trend that began with ln(ΔCO) = 8.1, so this is selected.
7/29	0.08	0.28	No decrease in ln(ΔCO) between these two transects (5.3) and at a different altitude (3800 m and 4500 m)
8/3 P1	0.11	0.81	Using Lagrangian transects following Wang et al. (2021)
8/3 P2	0.20	0.83	Youngest sampled age had a lower ln(ΔCO) at 7.7 than the second sampled (selected initialization transect) at 7.9
8/6	0.09	0.09	Removed the second sampled transect due to its ln(ΔCO) being higher than the others and not following a similar rate of decay.
8/7 P1	0.69	0.69	No change
8/7 P2	0.53	0.96	ln(ΔCO) of the youngest sampled was the lowest of all other transects sampled in this pass
8/12	0.75	0.78	Similar age and ln(ΔCO) for these two. Differed in diameter (140 nm and 150 nm) and in number concentration (16000 cm^{-3} and 58000 cm^{-3})

Table S3: Shown here are statistics on the various fits done in Figures 2 through 4. For rows where the left column is a rate of change ($\frac{d}{dt}$), the slope and intercept columns are an average from the Monte Carlo method of fitting based on the uncertainty of previously done linear regression. Statistically significant positive relationships are highlighted in red, while statistically significant negative relationships are highlighted in blue.

Fit	Slope	95% Confidence	Intercept	Intercept Confidence
Transect Average initial D_{pm} [nm] vs. log(ΔOA_i) [log(μg m^{-3})]	49.6	30.3 to 68.9	60.4	7.4 to 113.3
ΔCO Percentile initial D_{pm} [nm] vs. log(ΔOA_i) [log(μg m^{-3})]	40.3	32.2 to 48.5	90.7	69.5 to 111.8
Transect Average initial σ vs. log(ΔOA_i) [log(μg m^{-3})]	-0.06	-0.11 to -0.00	1.66	1.5 to 1.8
ΔCO Percentile initial σ vs. log(ΔOA_i) [log(μg m^{-3})]	-0.05	-0.07 to -0.03	1.63	1.6 to 1.7
Transect Average initial ΔN/ΔCO [cm^{-3} $ppbv^{-1}$] vs. log(ΔOA_i) [log(μg m^{-3})]	-40.3	-67 to -13	170	92 to 240
ΔCO Percentile initial ΔN/ΔCO [cm^{-3} $ppbv^{-1}$] vs. log(ΔOA_i) [log(μg m^{-3})]	-17.7	-31 to -4.0	98.8	63 to 134
Transect Average $\frac{dD_{pm}}{dt}$ [nm h^{-1}] vs. log(ΔOA_i) [log(μg m^{-3})]	4.3	1.1 to 7.9	-1.1	-9.9 to 7.5
ΔCO Percentile $\frac{dD_{pm}}{dt}$ [nm h^{-1}] vs. log(ΔOA_i) [log(μg m^{-3})]	3.9	2.2 to 5.5	0.6	-3.4 to 4.6
Transect Average $\frac{d\sigma}{dt}$ [h^{-1}] vs. log(ΔOA_i) [log(μg m^{-3})]	-0.01	-0.02 to -0.01	0.02	0.01 to 0.04
ΔCO Percentile $\frac{d\sigma}{dt}$ [h^{-1}] vs. log(ΔOA_i) [log(μg m^{-3})]	-0.01	-0.01 to -0.01	0.01	0.00 to 0.02
Transect Average $\frac{d(\Delta N/\Delta CO)}{dt}$ [cm^{-3} $ppbv^{-1}$ h^{-1}] vs. log(ΔOA_i) [log(μg m^{-3})]	-2.2	-12 to 7.7	-0.1	-32 to 31
ΔCO Percentile $\frac{d(\Delta N/\Delta CO)}{dt}$ [cm^{-3} $ppbv^{-1}$ h^{-1}] vs. log(ΔOA_i) [log(μg m^{-3})]	-4.4	-7.6 to -1.4	7.0	-2.5 to 17
Transect Average $OAER_i$ [μg m^{-3} $ppbv^{-1}$] vs. log(ΔOA_i) [log(μg m^{-3})]	0.17	0.10 to 0.25	-0.06	-0.26 to 0.14
ΔCO Percentile $OAER_i$ [μg m^{-3} $ppbv^{-1}$] vs. log(ΔOA_i) [log(μg m^{-3})]	0.12	0.08 to 0.17	0.09	-0.02 to 0.22
Transect Average $\frac{d(OAER)}{dt}$ [μg m^{-3} $ppbv^{-1}$ h^{-1}] vs. log(ΔOA_i) [log(μg m^{-3})]	-0.03	-0.06 to -0.01	0.08	0.03 to 0.13
ΔCO Percentile $\frac{d(OAER)}{dt}$ [μg m^{-3} $ppbv^{-1}$ h^{-1}] vs. log(ΔOA_i) [log(μg m^{-3})]	-0.02	-0.04 to -0.01	0.04	0.01 to 0.08
Transect Average $\Delta O{:}\Delta C_i$ vs. log(ΔOA_i) [log(μg m^{-3})]	-0.07	-0.11 to -0.02	0.59	0.48 to 0.71
ΔCO Percentile $\Delta O{:}\Delta C_i$ vs. log(ΔOA_i) [log(μg m^{-3})]	-0.06	-0.07 to -0.04	0.57	0.54 to 0.61
Transect Average $\frac{d(\Delta O:\Delta C)}{dt}$ [h^{-1}] vs. log(ΔOA_i) [log(μg m^{-3})]	-0.01	-0.02 to 0.01	0.07	0.03 to 0.1
ΔCO Percentile $\frac{d(\Delta O:\Delta C)}{dt}$ [h^{-1}] vs. log(ΔOA_i) [log(μg m^{-3})]	-0.00	-0.01 to 0.01	0.05	0.02 to 0.08

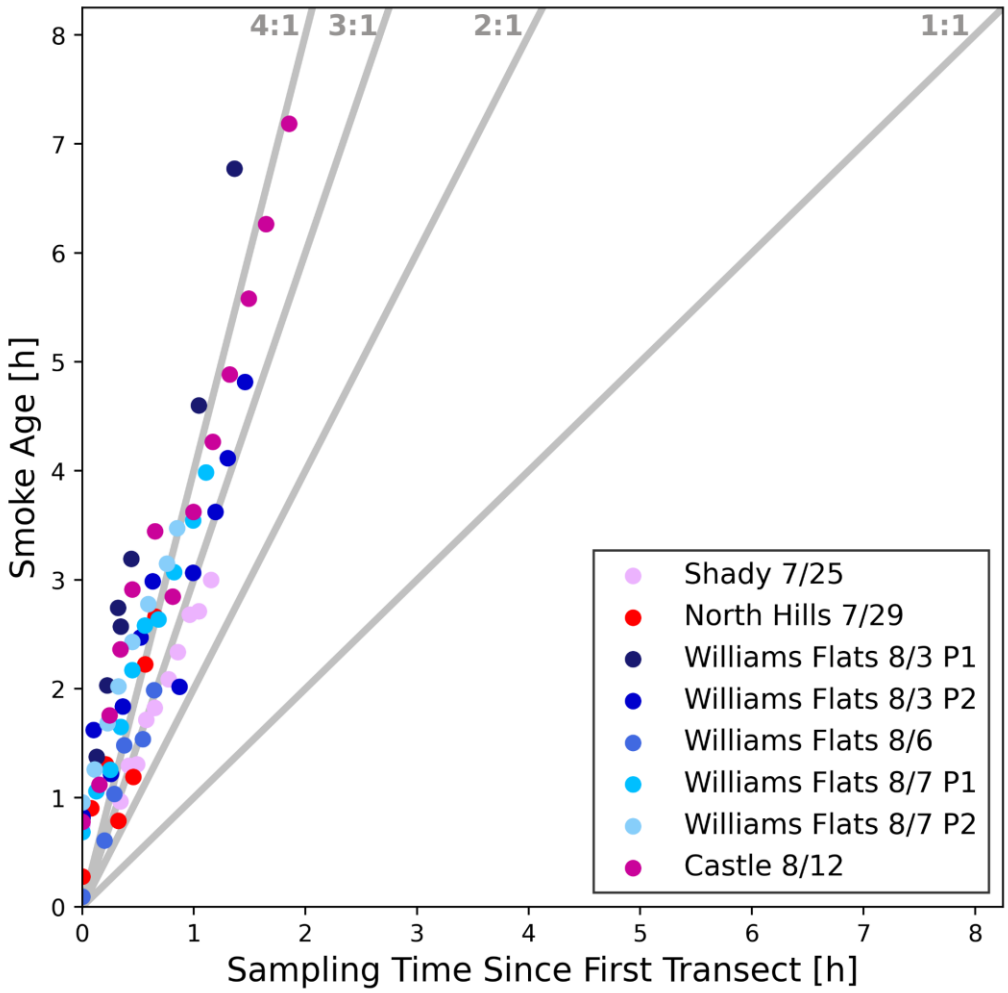

Figure S1: The physical smoke age versus the sampling time since the first transect in seconds for each of the eight sets of transects. The gray lines have slopes of 4, 3, 2 and 1, with the 1:1 line representing the ideal slope for Lagrangian sampling.

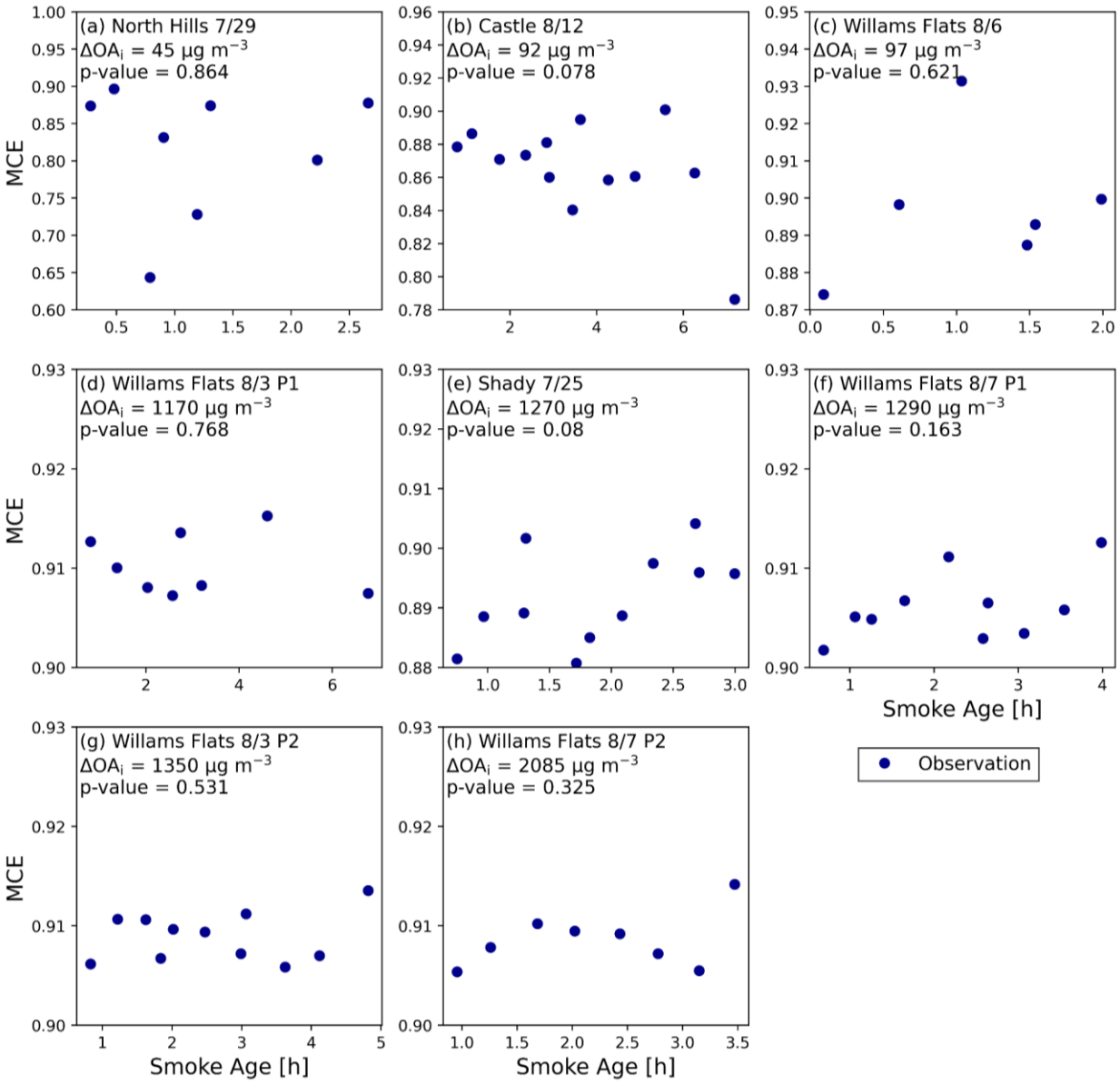

Figure S2: The modified combustion efficiency (MCE) versus smoke age for each of the eight flights, organized so that (a)-(h) are in order of increasing ΔOA_i. The in-plot text shows the ΔOA_i and the p-value of the linear regression of MCE with smoke age.

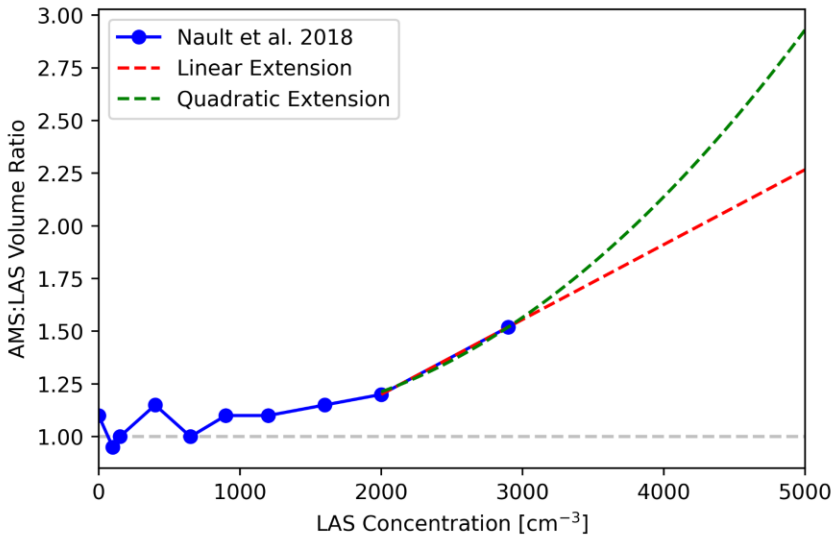

Figure S3: The AMS:LAS volume ratios versus LAS concentration used to saturation correct the LAS measurements. Below the LAS measurements of 2000 cm^{-3} with the impact of the dilution system of the instrument removed, results from Nault et al. 2018 (blue) are used to correct saturation. Above 2000 cm^{-3}, the linear extension (red dashed line) is used to saturation correct measurements at higher concentrations. Due to the uncertainty of what this function should be, correcting these higher concentrations with a quadratic extension (green dashed line) is also examined.

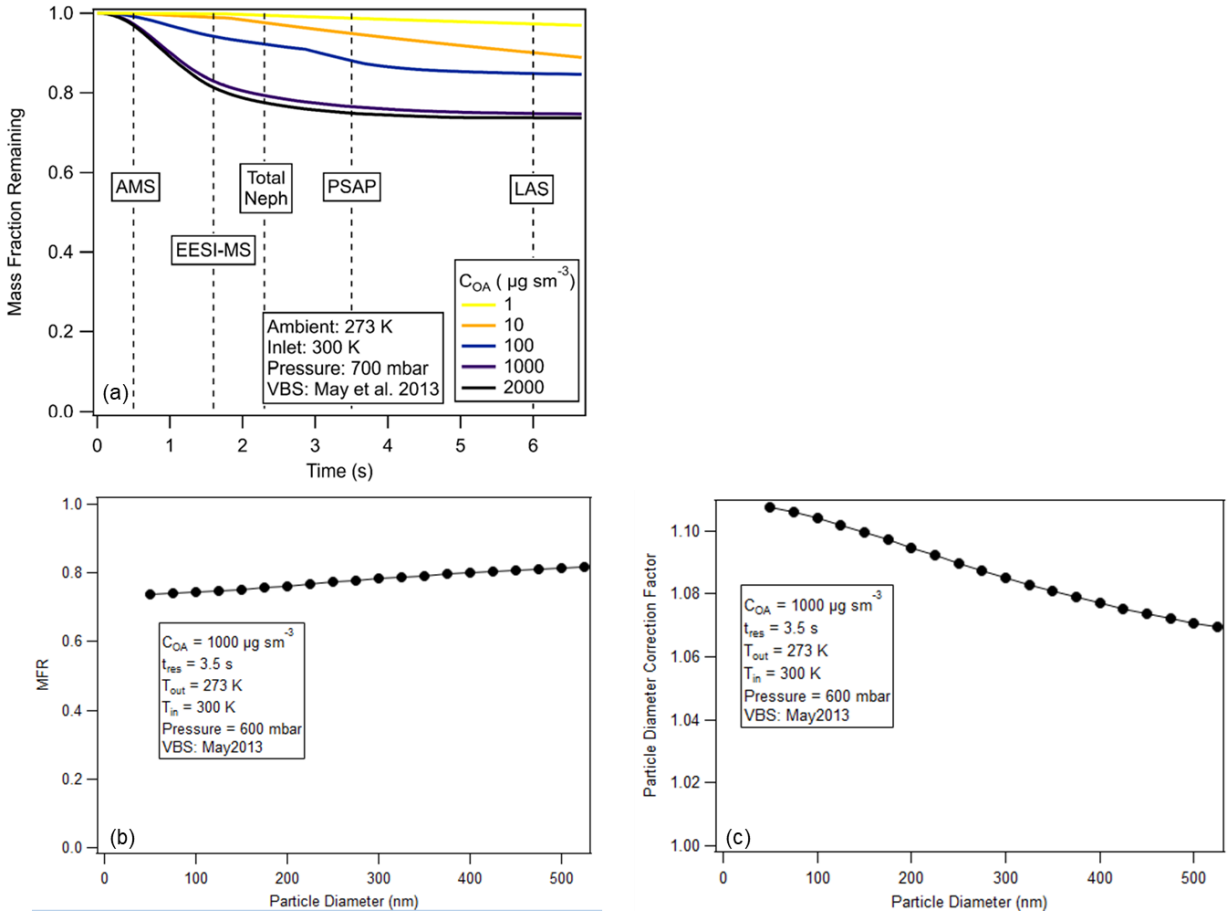

Figure S4: (a) The mass fraction remaining at each instrument for various concentrations of OA assuming a diameter of 300 nm, an ambient temperature of 273 K, and an inlet temperature of 300 K (Cappa, 2010; Pagonis et al., 2021). (b) An example of the size dependency of the mass fraction remaining (MFR), and (c) the correction factor for the particle diameter for an OA concentration of 1000 µg m^{-3}, an ambient temperature of 273 K, and an inlet temperature of 300 K.

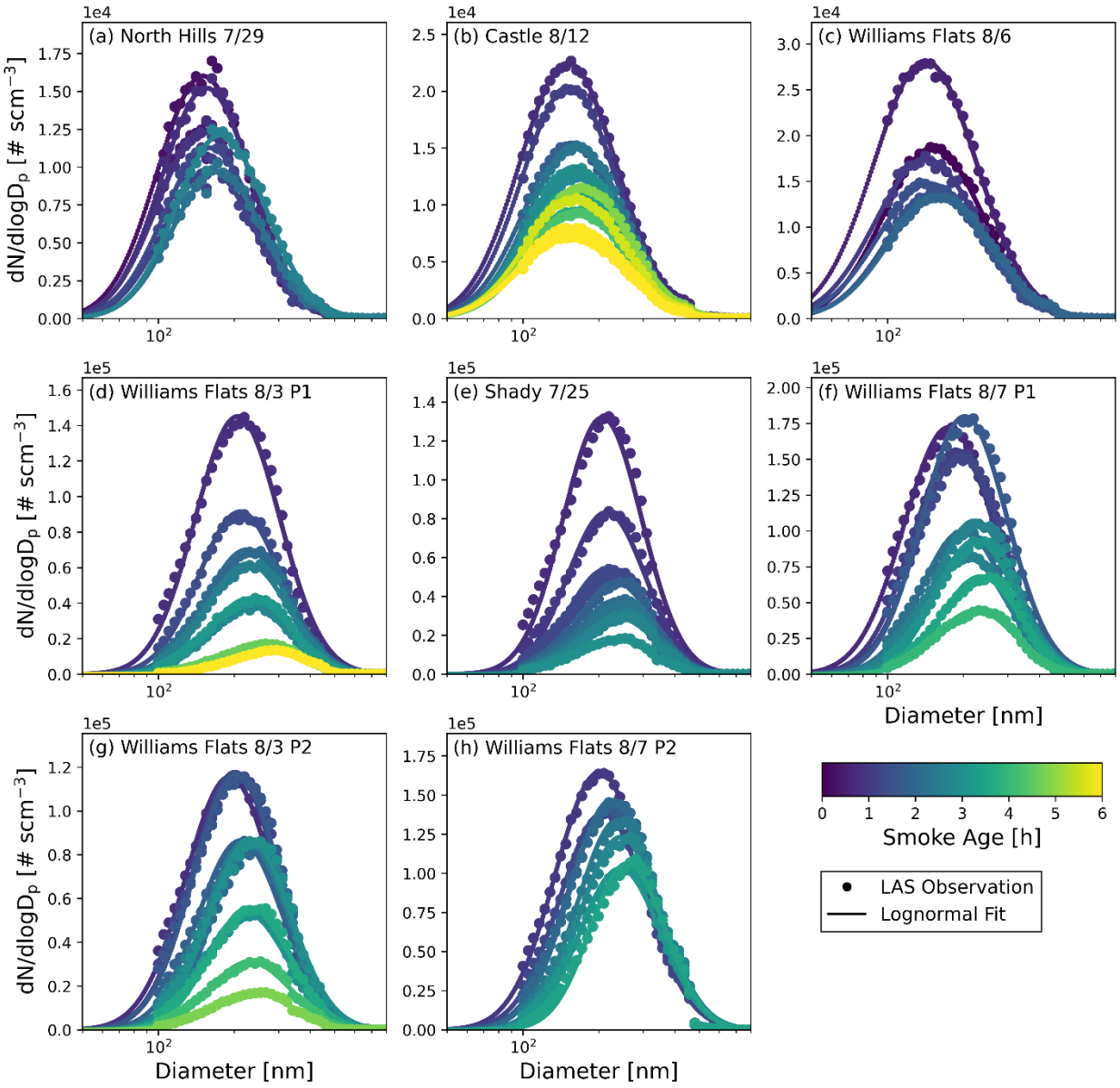

Figure S5: The lognormal fit of the LAS binned $dN/dlogD_p$ prior to corrections colored by smoke age for each set of transects.

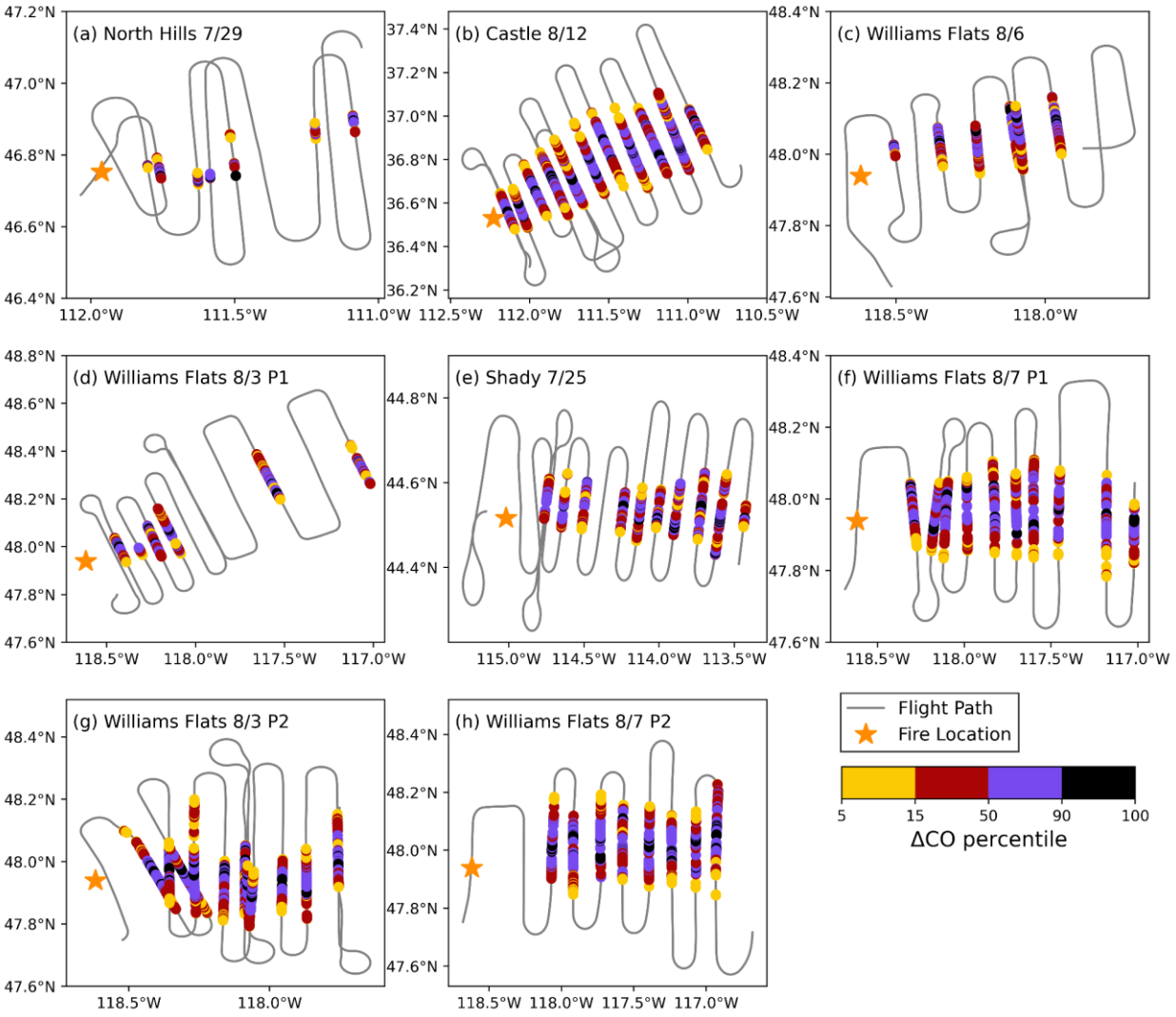

Figure S6: Flight tracks used in this study, with the location of the fire ignition shown as well. This location is not necessarily indicative of the location of fire emissions at the time of the DC8 sampling. The coloring is by ΔCO percentile, noting that the size of these percentile bins varies.

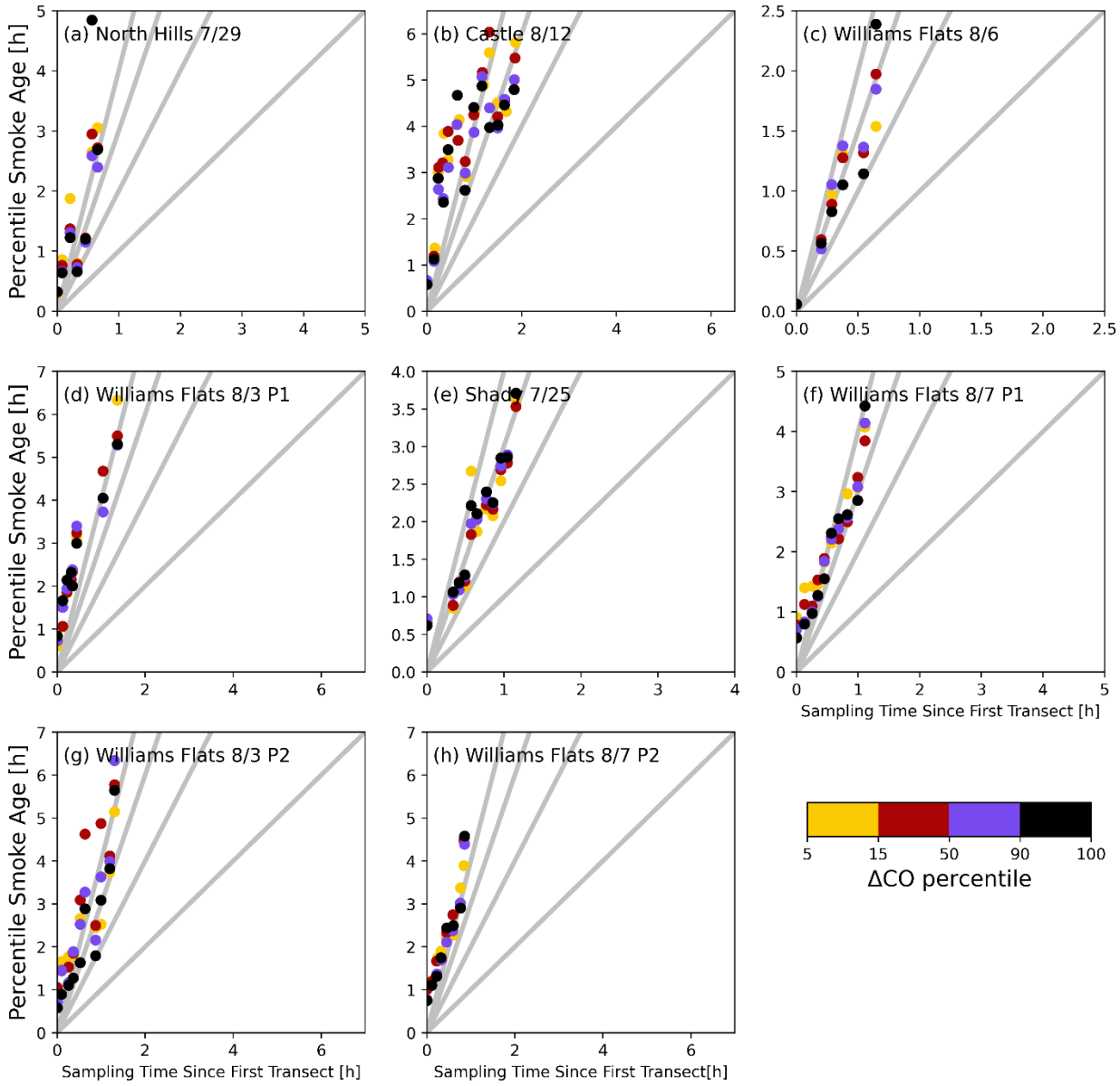

Figure S7: The physical smoke age in the percentiles versus the sampling time since the first transect in seconds for each of the eight sets of transects. The gray lines have slopes of 4, 3, 2 and 1, with the 1:1 line representing the ideal slope for Lagrangian sampling.

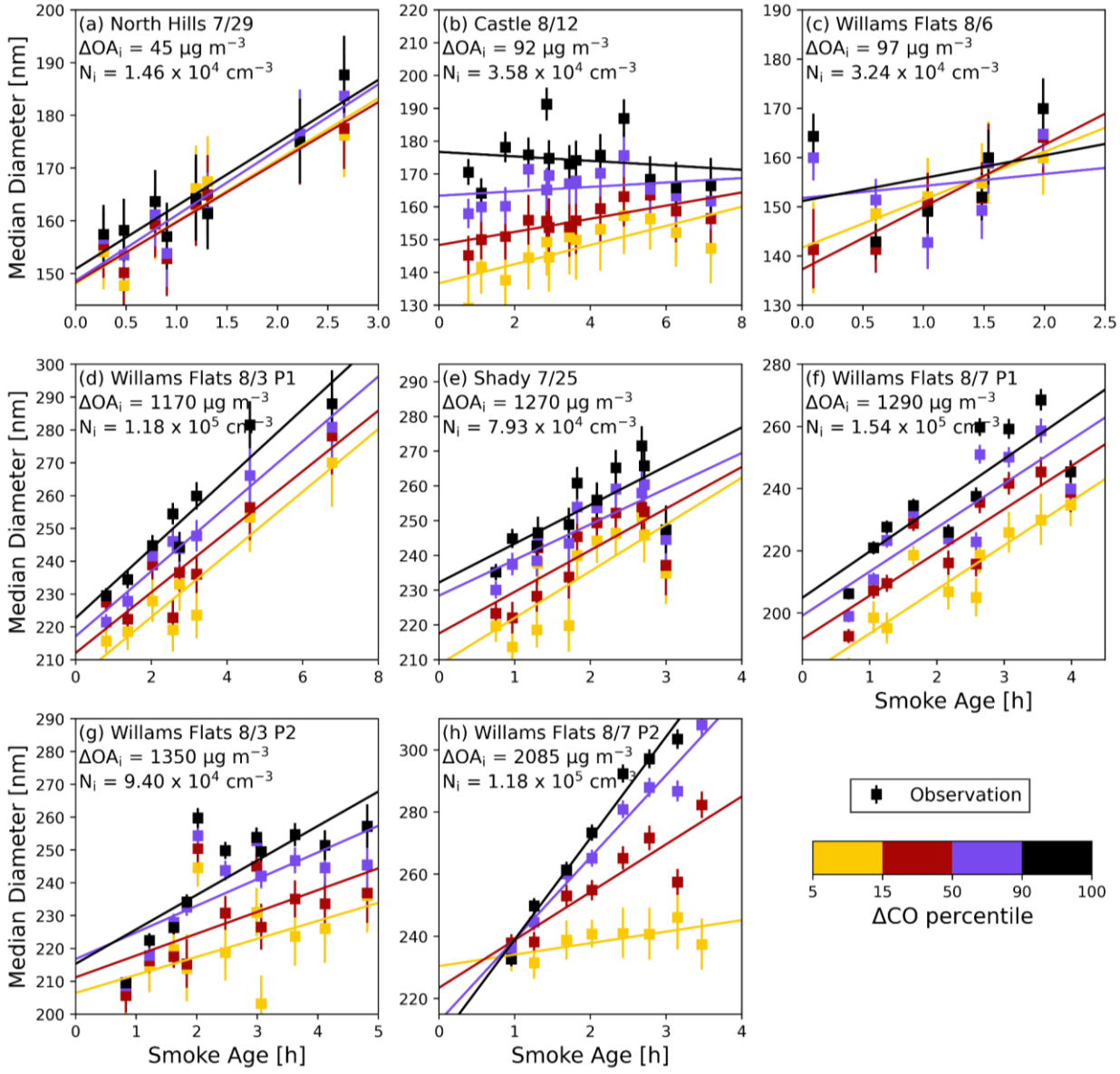

Figure S8: The median diameter (D_{pm}) versus smoke age for each of the eight flights, organized so that (a)-(h) are in order of increasing ΔOA_i. The color shows the percentile bin for each transect. The error bars represent the standard deviation of D_{pm} within the transect for each percentile bin.

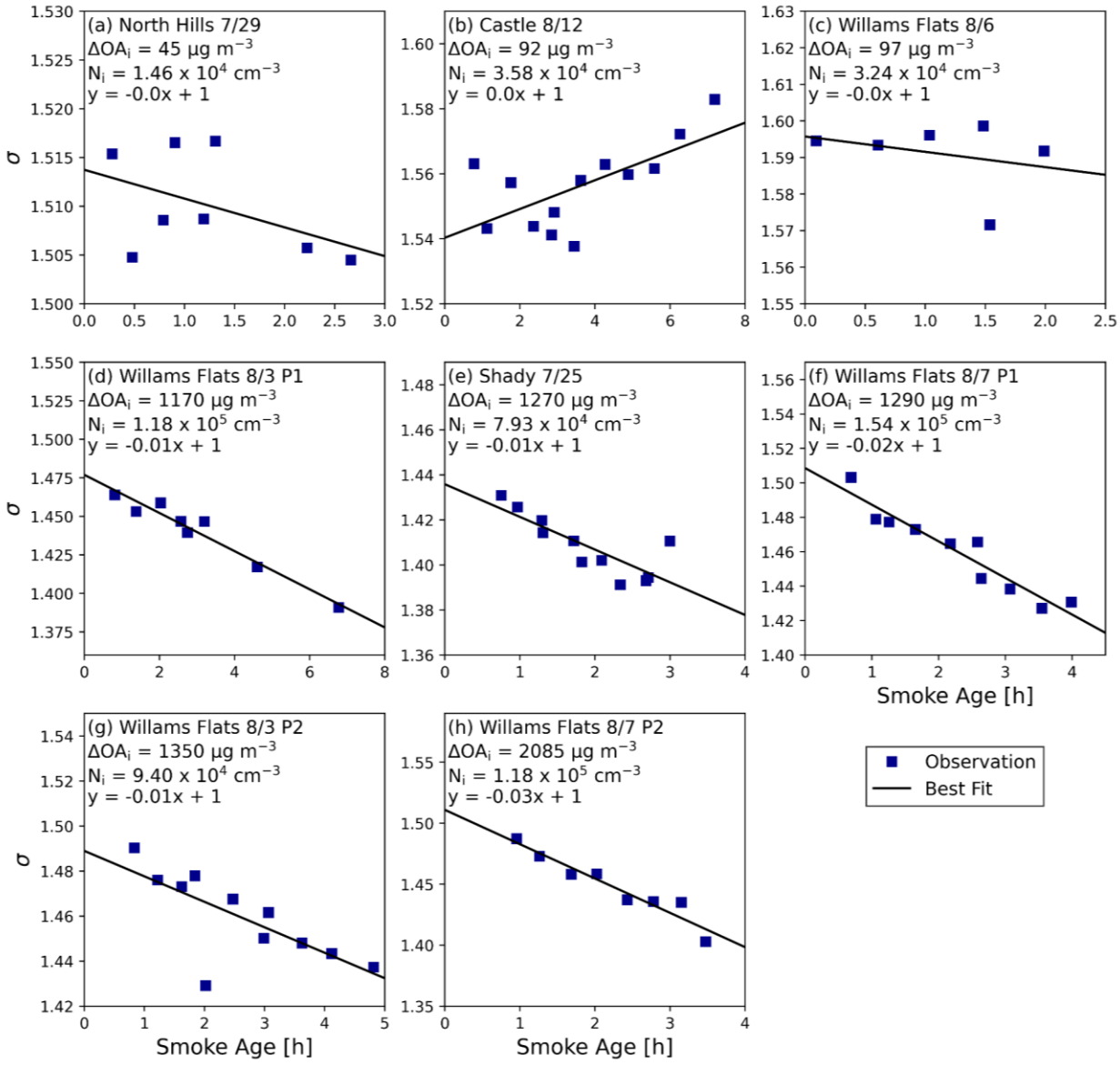

Figure S9: The modal width of the aerosol size distribution (σ) versus smoke age for each of the eight flights, organized so that (a)-(h) are in order of increasing ΔOA_i.

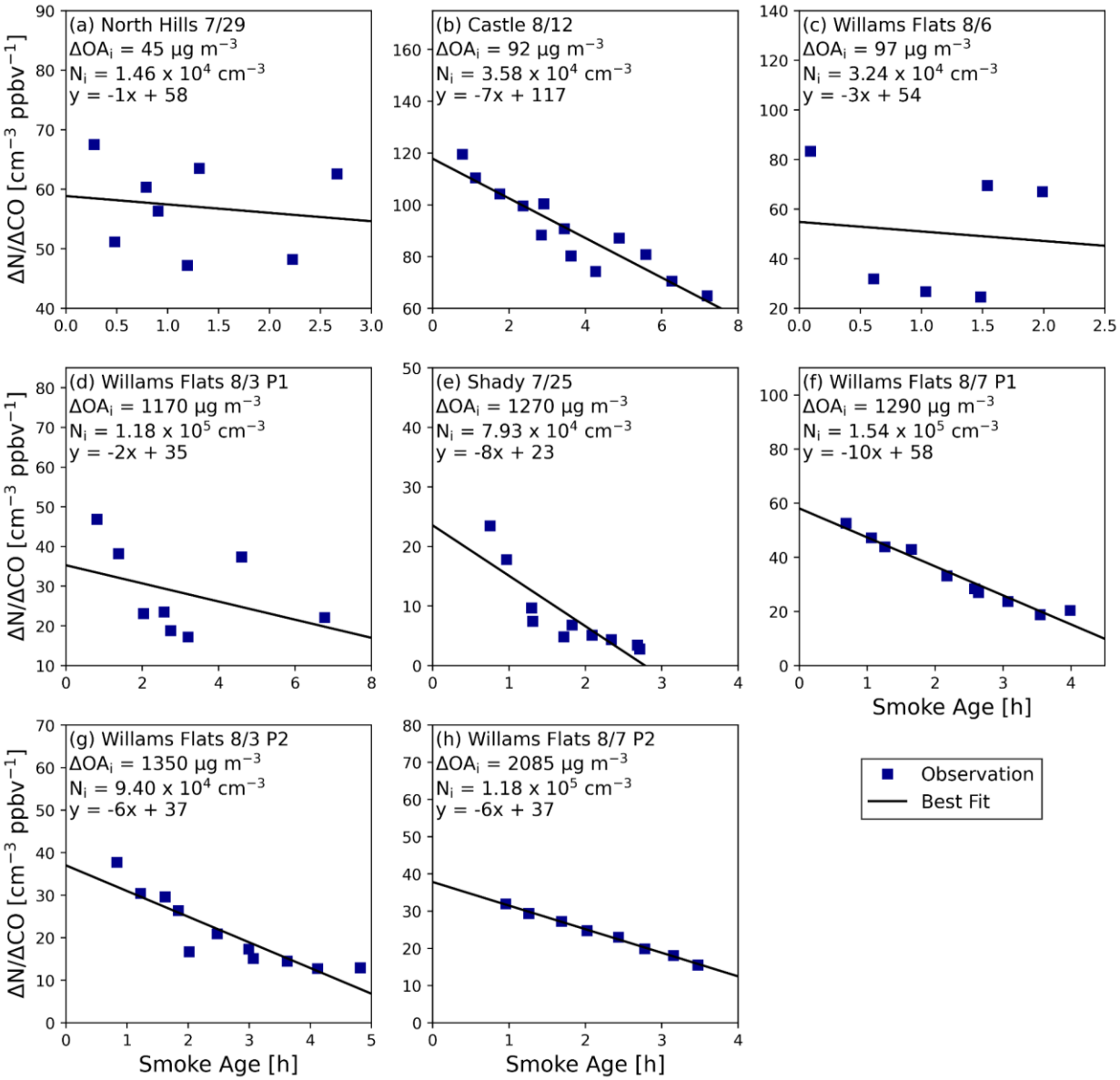

Figure S10: The number enhancement ratio (ΔN/ΔCO) versus smoke age for each of the eight flights, organized so that (a)-(h) are in order of increasing ΔOA_i.

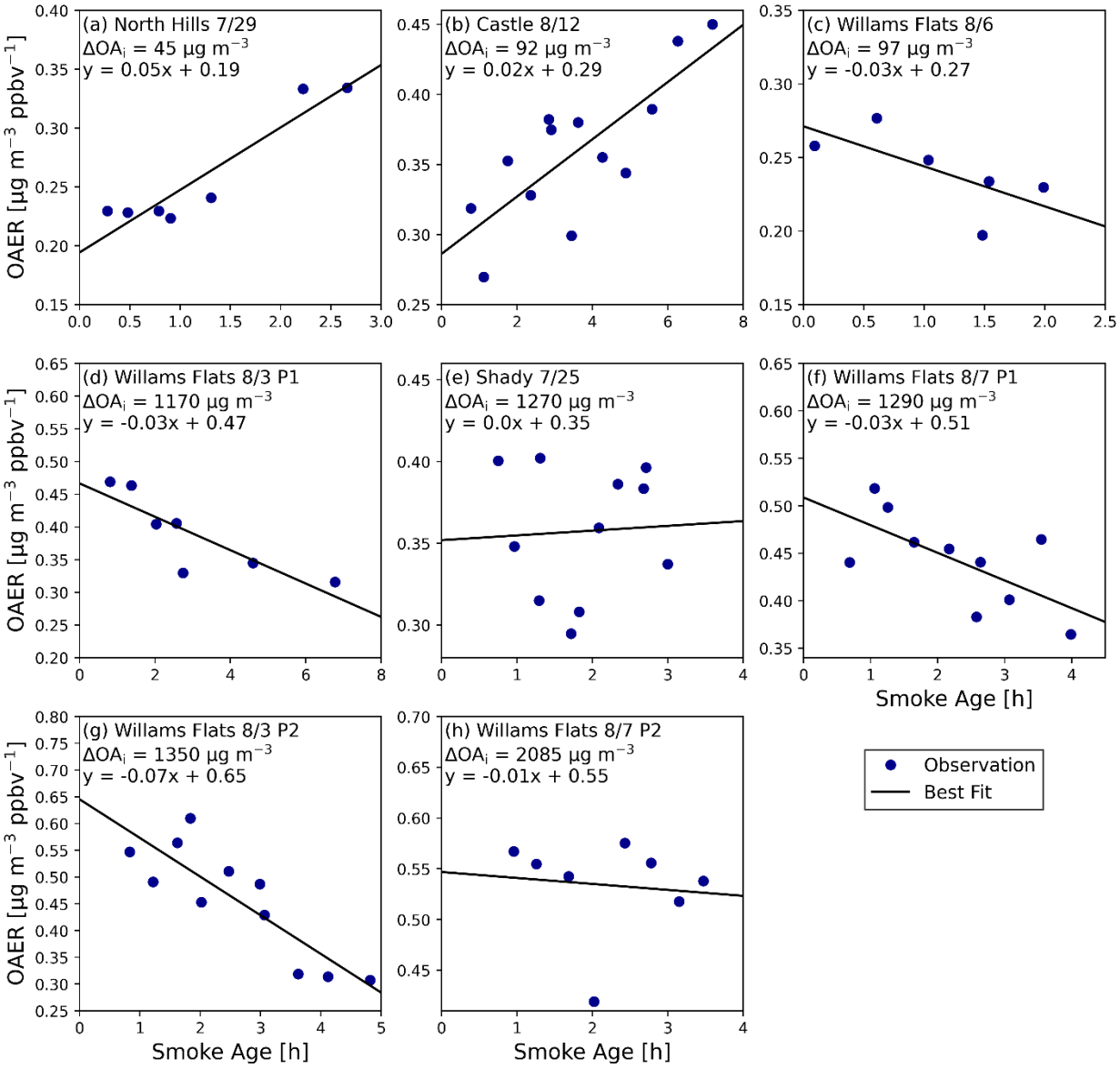

Figure S11: The organic aerosol excess mixing ratio (OAER) versus smoke age for each of the eight flights, organized so that (a)-(h) are in order of increasing ΔOA_i.

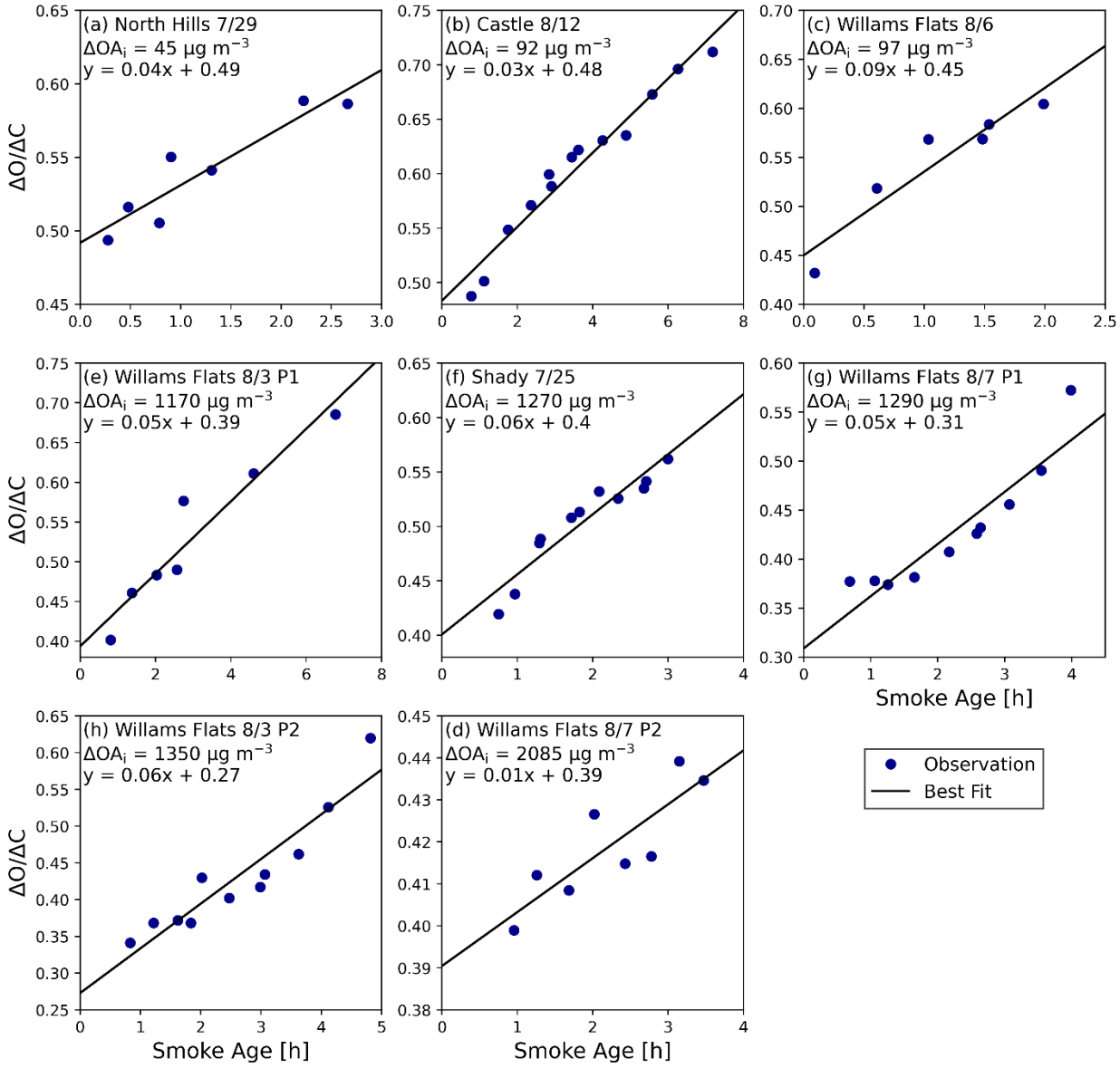

Figure S12: The ΔO:ΔC versus smoke age for each of the eight flights, organized so that (a)-(h) are in order of increasing ΔOA_i.

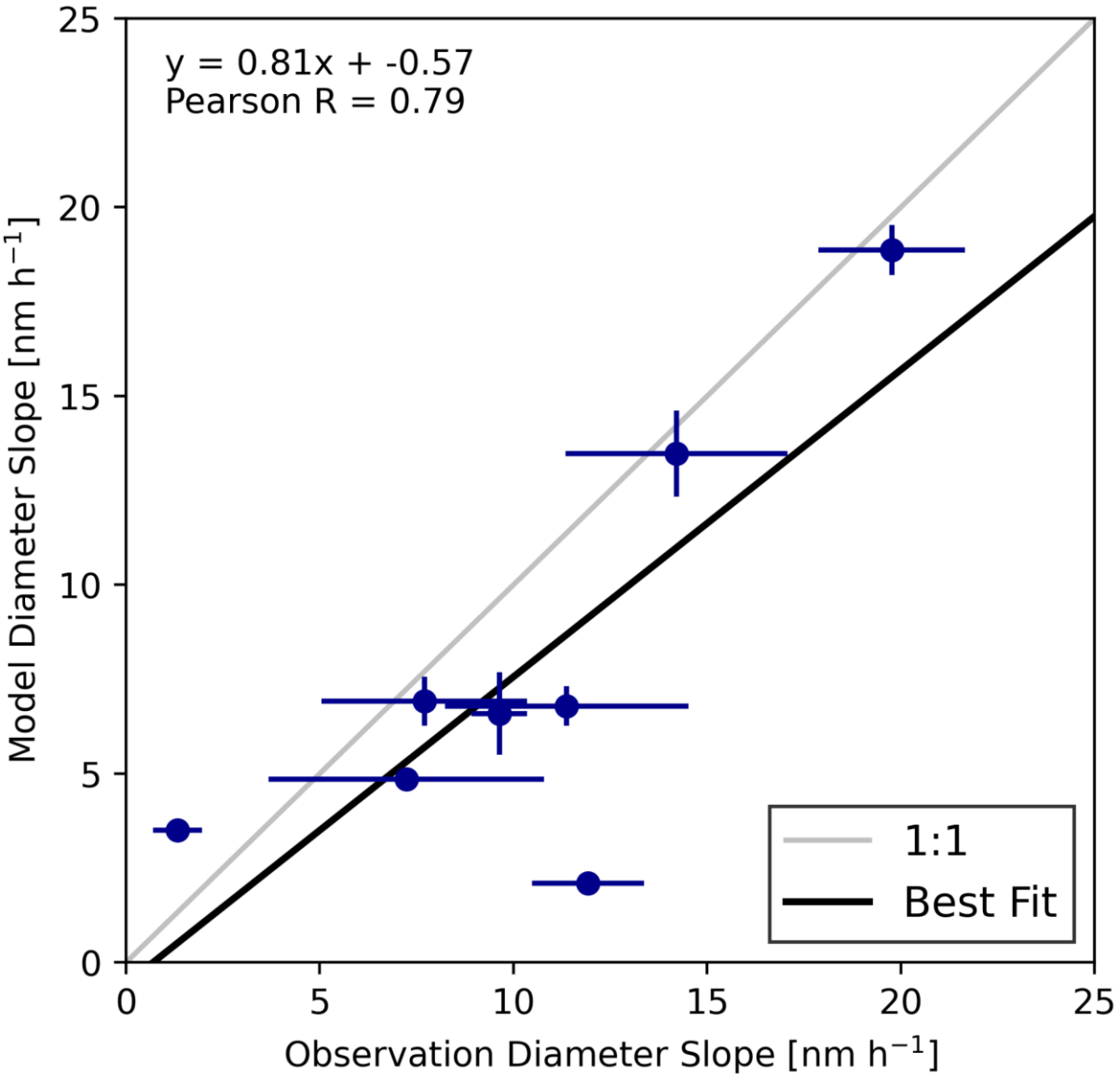

Figure S13: The modeled rate of change of median diameter with smoke age versus the observed rate of change of median diameter with smoke age. The error bars represent the respective 95% confidence intervals of the rates of change. The black line is the 1:1 line, and the gray line is the linear regression.

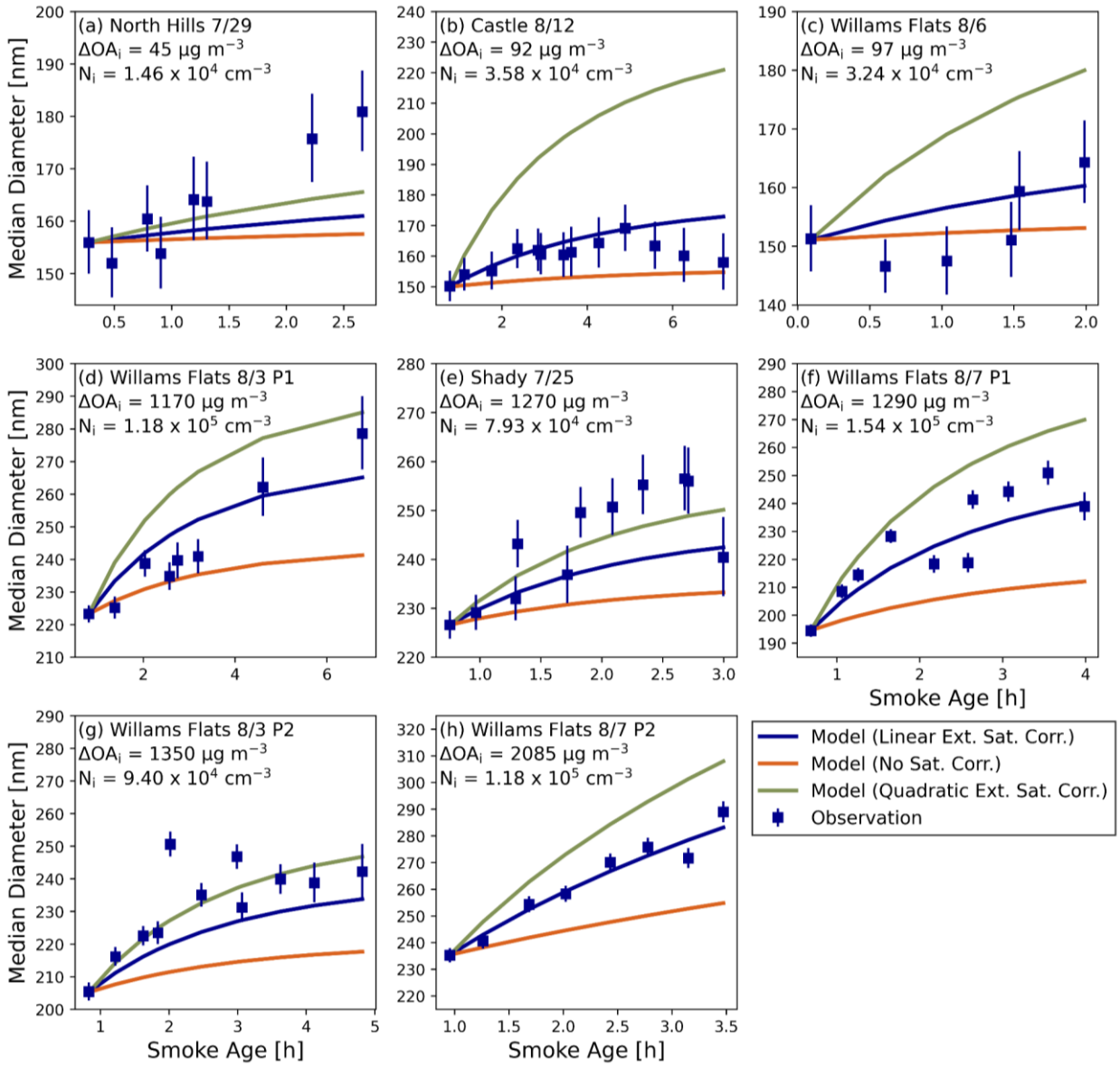

Figure S14: The transect averaged observed median diameter, along with the simulated median diameter with coagulation and dilution based on either no saturation correction (orange), a linear extended saturation correction (blue), or a quadratic extended saturation correction (green). The error bars represent the standard deviation of D_p within the transect. (a) to (h) are organized in order of increasing ΔOA_i.

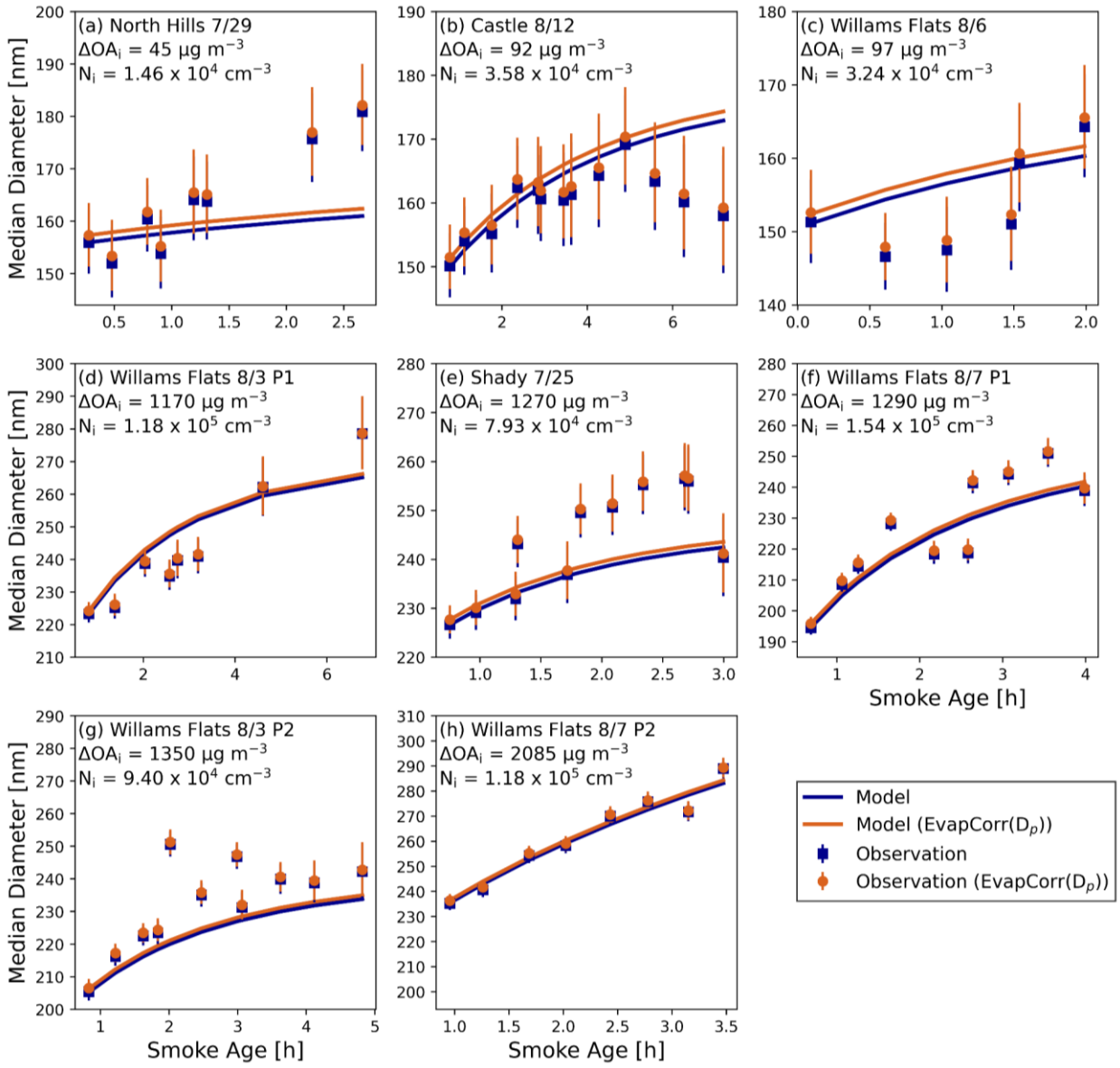

Figure S15: The observed and coagulation simulated transect averaged median diameter as a function of smoke age with the LAS evaporation correction having no size dependency (blue), and with the evaporation correction for the LAS having a size dependency (orange). The error bars represent the standard deviation of D_p within the transect. (a) to (h) are organized in order of increasing ΔOA_i.

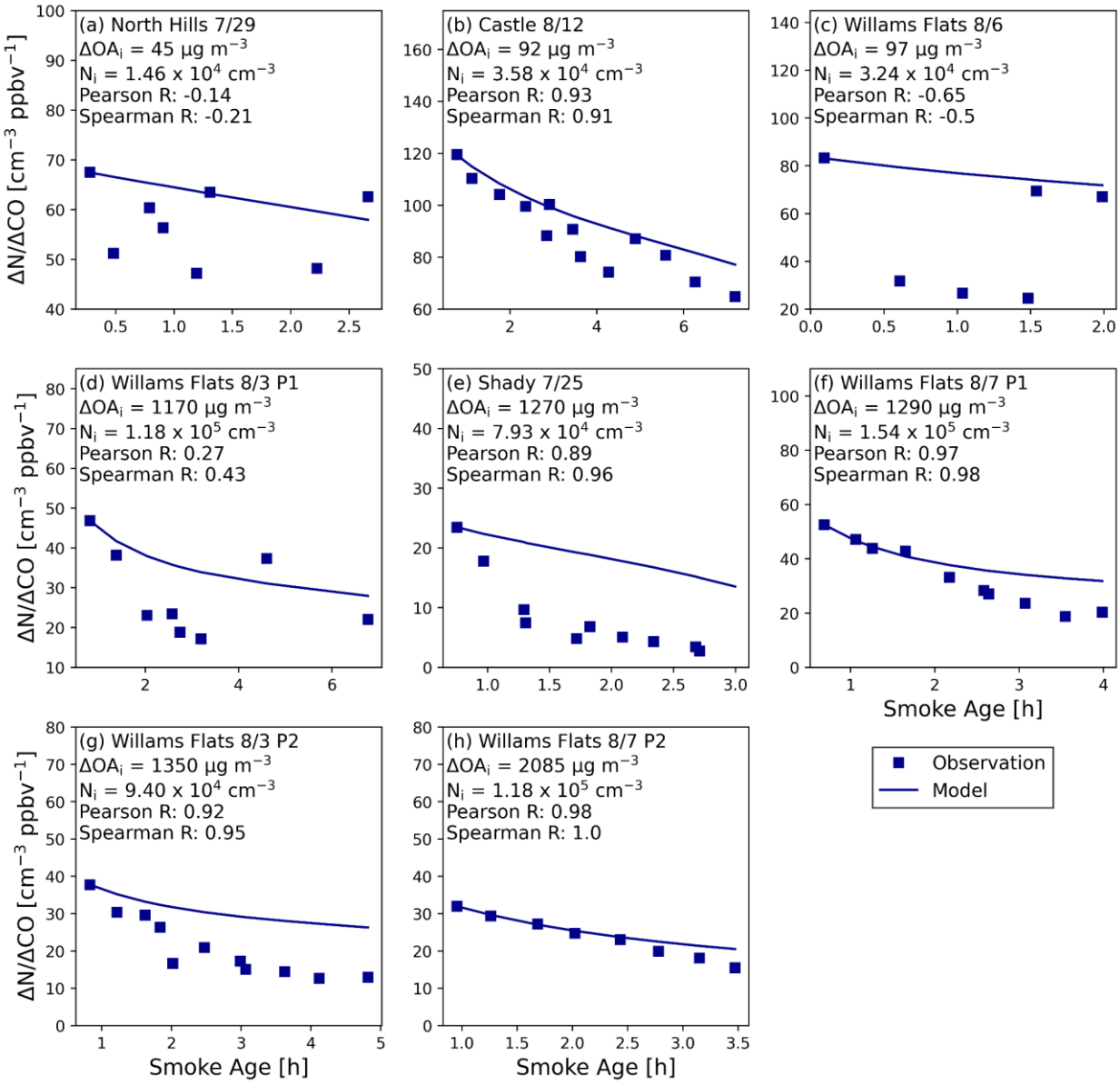

Figure S16: The observed and simulated number enhancement ratio (ΔN/ΔCO) with smoke age for each of the eight sets of transects, with (a) to (h) organized in order of increasing ΔOA$_i$.

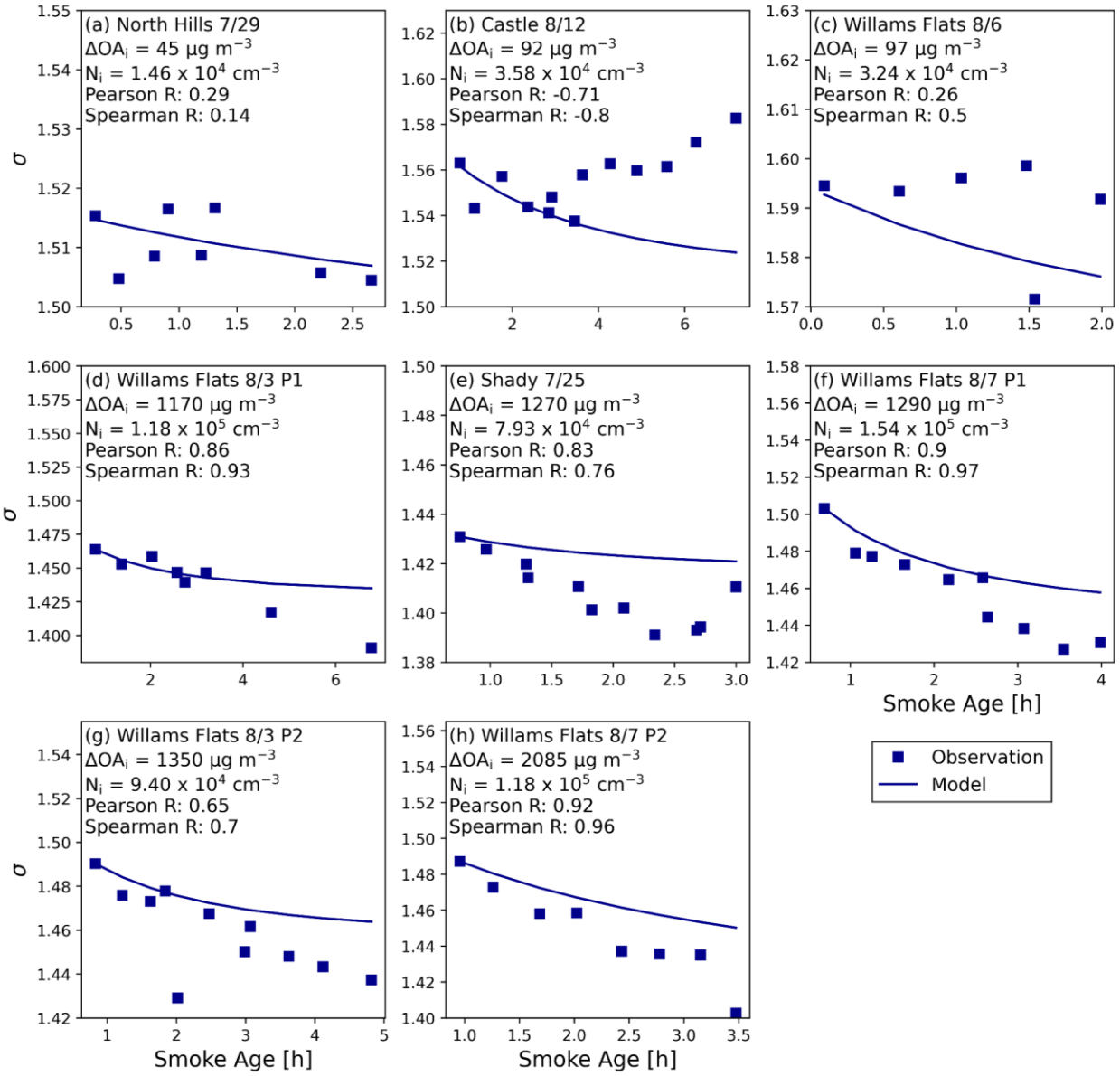

Figure S17: The observed and simulated modal width of the aerosol size distribution (σ) with smoke age for each of the eight sets of transects, with (a) to (h) organized in order of increasing ΔOA_i.

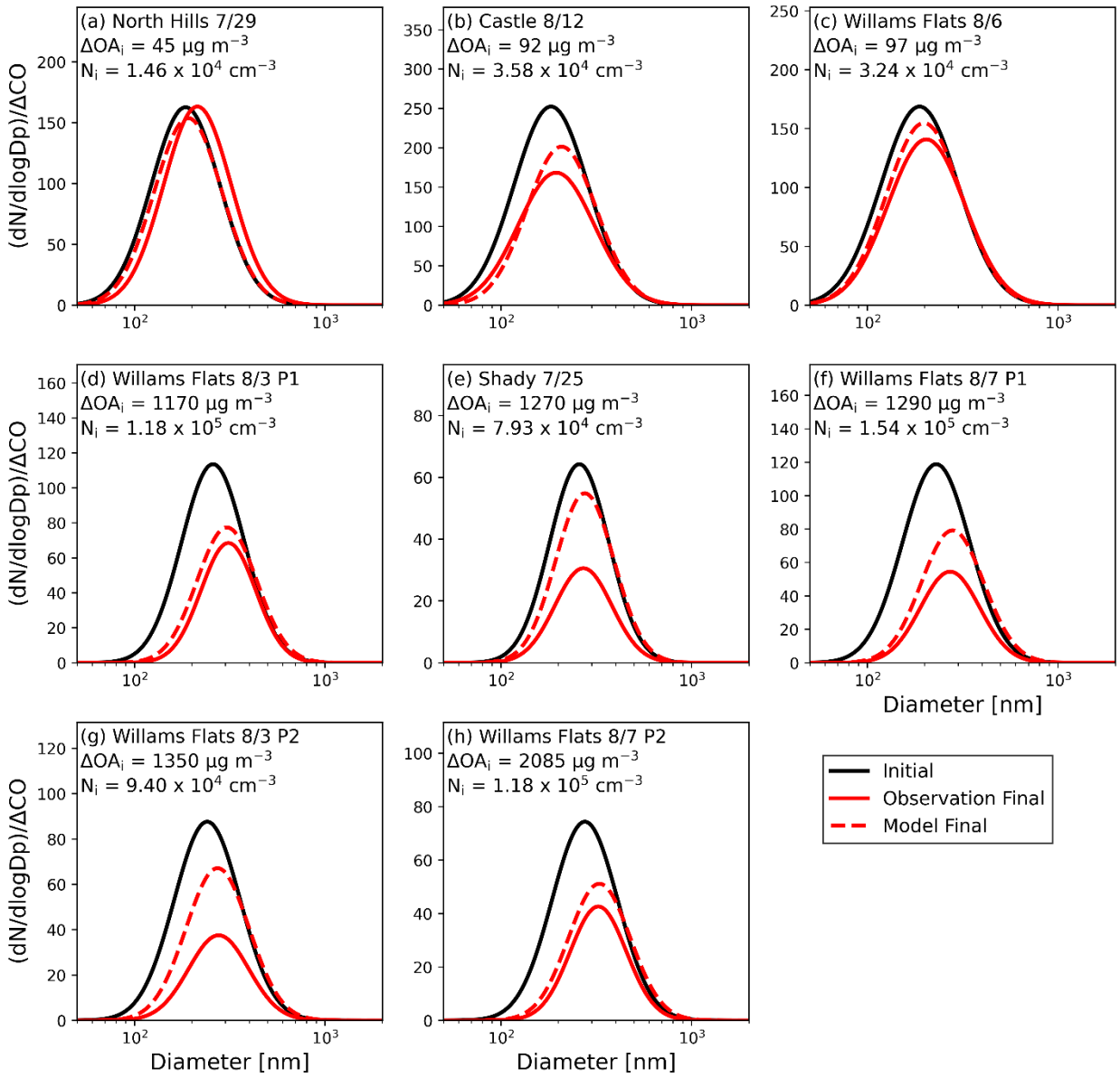

Figure S18: Normalized dN/dlogDp in the model and observations at the first transect and final transect, with (a) to (h) organized in order of increasing ΔOA_i.

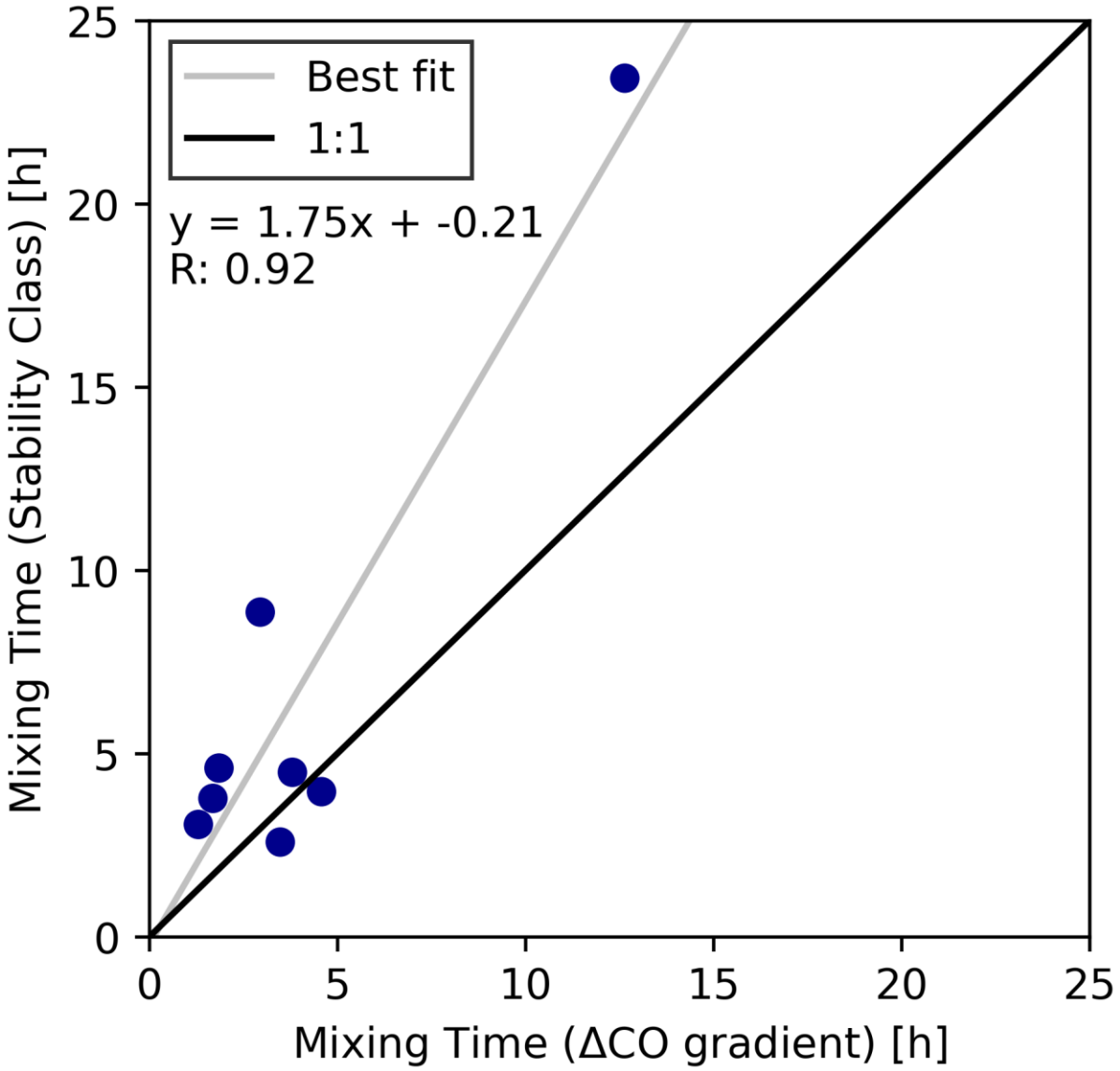

Figure S19: The mixing time calculated from stability classes derived from the standard deviations in the wind versus a mixing time based on the rate of change of the ΔCO gradient between the core and edge regions. These methods are described in Sect. 2.1.2.